AGU PUBLICATIONS

Geophysical Research Letters

RESEARCH LETTER
10.1002/2014GL060707

Key Points:
- Discrete emissions are generated nonlinearly with optimum conditions
- For hiss-like emissions, both occurrence rate and amplitudes increase with Nh/Nt
- The discrete emissions likely occur with a limited range in Nh/Nt and Bw

Correspondence to:
X. Gao,
gaoxl@mail.ustc.edu.cn

Citation:
Gao, X., W. Li, R. M. Thorne, J. Bortnik, V. Angelopoulos, Q. Lu, X. Tao, and S. Wang (2014), New evidence for generation mechanisms of discrete and hiss-like whistler mode waves, *Geophys. Res. Lett.*, *41*, 4805–4811, doi:10.1002/2014GL060707.

Received 29 MAY 2014
Accepted 27 JUN 2014
Accepted article online 30 JUN 2014
Published online 16 JUL 2014

New evidence for generation mechanisms of discrete and hiss-like whistler mode waves

Xinliang Gao[1,2], Wen Li[2], Richard M. Thorne[2], Jacob Bortnik[2], Vassilis Angelopoulos[3], Quanming Lu[1], Xin Tao[1], and Shui Wang[1]

[1]CAS Key Laboratory of Geospace Environment, Department of Geophysics and Planetary Science, University of Science and Technology of China, Hefei, China, [2]Department of Atmospheric and Oceanic Sciences, University of California, Los Angeles, California, USA, [3]Institute of Geophysics and Planetary Physics/Department of Earth, Planetary, and Space Sciences, University of California, Los Angeles, California, USA

Abstract Linear theory suggests that whistler mode wave growth rates are proportional to the ratio of hot electron (~1 to 30 keV) density to total electron density (N_h/N_t), whereas nonlinear wave theory suggests that an optimum linear growth rate is required to generate rising tone chorus from hiss-like emissions. Using the Time History of Events and Macroscale Interactions during Substorms waveform data collected by three probes over the past ~5 years, we investigate the correlation between N_h/N_t and wave amplitude/wave occurrence rate for rising tone, falling tone, and hiss-like emissions separately. Statistical results show that the rising and falling tones preferentially occur in the region with a limited N_h/N_t range, whereas both the occurrence rate and wave amplitudes of hiss-like emissions become larger for higher values of N_h/N_t. Our statistical results not only provide an important clue on the generation mechanism of hiss-like emissions, but also provide supporting experimental evidence for the nonlinear theory of generating rising tone chorus.

1. Introduction

Whistler mode waves are intense electromagnetic emissions that occur ubiquitously in the Earth's inner magnetosphere, typically in two distinct frequency bands: a lower band (0.1–0.5 f_{ce}, where f_{ce} is the electron gyrofrequency) and an upper band (0.5–0.8 f_{ce}) with a gap in wave power at 0.5 f_{ce} [*Burtis and Helliwell*, 1969; *Tsurutani and Smith*, 1974, 1977; *Koons and Roeder*, 1990; *Meredith et al*., 2001; *Li et al*., 2012]. The whistler mode wave emissions are generally believed to be excited in the vicinity of the geomagnetic equatorial plane [*LeDocq et al*., 1998; *Lauben et al*., 2002; *Santolik et al*., 2005; *Li et al*., 2009], but another source region may also be present at high latitudes in the dayside magnetosphere [*Tsurutani and Smith*, 1977; *Tsurutani et al*., 2009]. Because they provide efficient energy diffusion through cyclotron resonances, whistler mode waves are fundamentally important for accelerating seed electrons to highly relativistic energies [*Summers et al*., 1998; *Meredith et al*., 2001; *Horne et al*., 2005; *Cattell et al*., 2008; *Thorne et al*., 2013]. On the other hand, they can also scatter electrons into the loss cone leading to precipitation into the upper atmosphere, which is an important loss process in the radiation belts and provides a major source of energy for the diffuse and pulsating aurora [*Horne and Thorne*, 2003; *Ni et al*., 2008, 2011; *Nishimura et al*., 2010, 2013; *Thorne et al*., 2005, 2010].

The generation mechanism of whistler mode emissions in the magnetosphere has been a long-standing problem and received intense attention but has not yet been fully understood. The theory of *Kennel and Petschek* [1966], who evaluated linear growth rates for weakly growing whistler mode waves, works well for evaluating the linear phase of whistler mode wave instability [e.g., *Li et al*., 2009]. However, nonlinear theory is required to explain the generation of discrete rising tone chorus [*Omura et al*., 2008; *Omura and Nunn*, 2011]. The essential feature of nonlinear theory is the resonant current formed by the electromagnetic electron hole in the velocity phase space [*Omura et al*., 2008]. However, direct observational evidence of this electron hole, which rotates with the local electron gyrofrequency, is far beyond the detection capability of current particle instruments. Another possible way to test the theory is to compare the observed frequency sweep rates with those obtained from the theory. *Cully et al*. [2011] showed good agreement between frequency sweep rates observed by the Time History of Events and Macroscale Interactions during Substorms (THEMIS) probes and those obtained from the nonlinear wave growth theory. However, *Tao et al*. [2012] found that the sweep rates observed from THEMIS can also be well predicted by alternate theories proposed by *Helliwell* [1967] and *Trakhtengerts* [1995]. Therefore, more observational evidence is still needed to test these nonlinear wave excitation theories.

The nonlinear wave growth theory also suggested that an optimum amplitude of the triggering waves is a key parameter to generate rising tone chorus emissions [*Omura and Nunn*, 2011]. More recently, *Hikishima and Omura* [2012] have confirmed this optimum wave amplitude condition by performing a self-consistent electromagnetic particle simulation. In their simulation, the rising tone emissions can only be generated if the initial wave amplitude of triggering emissions is close to the optimum wave amplitude. The triggering emission injected in their simulation to generate rising tone chorus is similar to the waves generated from the thermal noise by linear instability. Therefore, we expect that initial linear growth rate is closely related to whether the rising tone chorus can be generated from the hiss-like emissions.

Since the ratio of the hot electron (~1 to 30 keV) density to the total electron density (N_h/N_t) is proportional to the linear growth rate [*Kennel and Petschek*, 1966], in the present paper, we evaluate the correlation between the N_h/N_t and the wave amplitude/occurrence for discrete (rising or falling tones) elements and hiss-like emissions separately. By analyzing ~5 years of the THEMIS waveform data and the corresponding value of N_h/N_t, we attempt to test these linear and nonlinear wave generation mechanisms for whistler mode waves.

2. THEMIS Data Analysis

The THEMIS spacecraft with apogees above 10 R_E and perigees below 2 R_E [*Angelopoulos*, 2008] is well suited to measure whistler mode emissions in the near-equatorial magnetosphere. These whistler mode waves can be measured by the Search-Coil Magnetometer (SCM) [*Le Contel et al*., 2008; *Roux et al*., 2008] and Electric Field Instrument (EFI) [*Bonnell et al*., 2008]. Several waveform bursts, each lasting about 6–8 s, are recorded per day simultaneously from SCM and EFI with a sampling frequency of up to ~16 kHz. Wave bursts have not been triggered completely randomly, but this will not affect our essential conclusion since we investigate the relative occurrence of each type of emission. The magnetic wave burst data are mainly utilized to analyze the polarization properties of the whistler mode waves. The background magnetic field intensity measured by the fluxgate magnetometer (FGM) [*Auster et al*., 2008] is used to calculate the electron gyrofrequency. The hot electron density is obtained from the electrostatic analyzer (ESA) instrument [*McFadden et al*., 2008], which can measure electron distributions from several eV to ~30 keV. The total electron density is inferred from the spacecraft potential and the electron thermal speed measured by the EFI and ESA instruments, respectively [*Li et al*., 2010]. In our data set, we exclude the whistler mode waves observed outside the magnetopause or inside the plasmapause following the method described by *Li et al*. [2010].

Following the procedure developed by *Bortnik et al*. [2007] (essentially an implementation of *Means* [1972]), we analyze the three components of magnetic fields (rotated into the field-aligned coordinate system) from wave burst data to obtain the polarization parameters of whistler mode waves. These calculated wave polarization parameters have a time resolution of ~0.032 s, which is much shorter than the typical temporal duration of each discrete chorus element (a few tenths of seconds [e.g., *Cully et al*., 2008; *Santolik et al*., 2008; *Macusova et al*., 2010]). The high polarization ratio (R_p), defined as the ratio of polarized power to total power, indicates the high reliability of the calculated wave polarization parameters [*Bortnik et al*., 2007]. Since the whistler mode waves typically have large polarization ratios and ellipticities close to ~1, we only record wave polarization parameters when $R_p > 0.9$ and ellipticity > 0.7 [e.g., *Tsurutani et al*., 2009]. Because only the magnetic fields are analyzed in the procedure, there is an inherent 180° ambiguity in the wave normal direction. Therefore, we convert all the wave normal directions into values less than 90°.

3. Observational Results

During the period from 1 June 2008 to 1 June 2013, all the waveform data from the three inner probes (THEMIS A, D, and E) between 5 and 10 R_E are included in our data set of whistler mode wave emissions. Note that we only focus on analyzing lower band waves in the present study. Whistler mode waves in the inner magnetosphere exhibit three kinds of structure when shown in the frequency-time spectrogram: rising tones, falling tones, and hiss-like emissions. Representative examples of a rising tone, a falling tone, and a hiss-like emission are given in Figure 1. The top row shows a flag, which is used to identify whether the whistler mode emissions are rising tones (flag = 1), falling tones (flag = −1), or hiss-like emissions (flag = 0), and the flag is set to "*NaN*" if whistler mode waves are not detected. For each wave event, at one recording time, if the maximum magnetic spectral density between 0.1 and 0.5 f_{ce} is smaller than 1% of the maximum magnetic spectral density of this entire wave event, we assume that whistler mode waves are not detected at

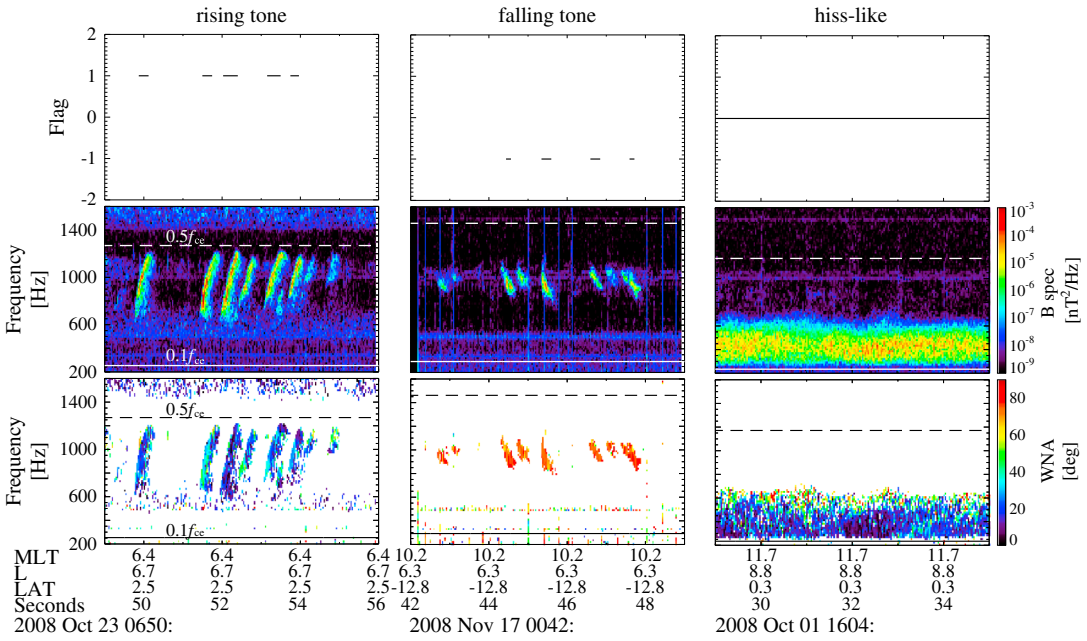

Figure 1. (top row) A flag used to classify the emission, (middle row) the frequency-time spectral density of the wave magnetic field, and (bottom row) the wave normal angle for three wave events: (first column) rising tones, (second column) falling tones, and (third column) hiss-like emissions, respectively. In the last two rows, the solid and dashed horizontal lines in white or black represent 0.1 and 0.5 f_{ce}, respectively.

this time. At each recording time (with the time resolution of 0.032 s), the frequency corresponding to the maximum magnetic spectral density is recorded after smoothing the adjacent three points in frequency. Then we calculate the frequency sweep rate using the five adjacent points in time. If the sign of the frequency sweep rate remains positive (or negative) for longer than 0.1 s, the flag is set to 1 (or −1); otherwise, it is set to 0. This procedure is similar to that of *Li et al.* [2012]. As shown in the bottom row, the rising tone and hiss-like emission are nearly field aligned, while the falling tone is very oblique. These results are consistent with those shown by *Li et al.* [2012].

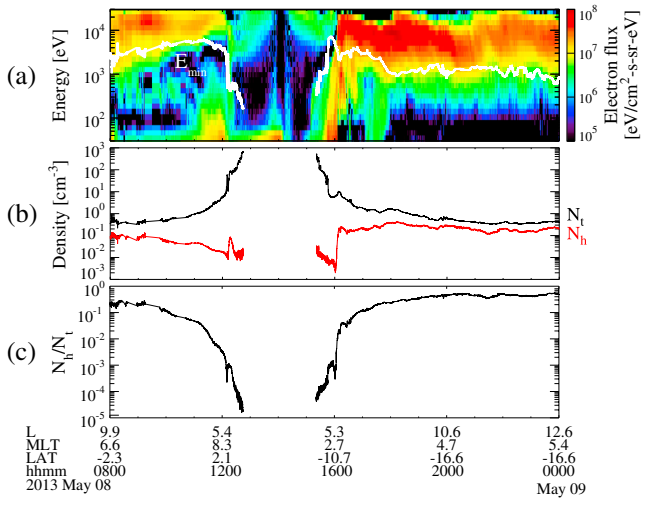

Figure 2. Time evolution of (a) the electron energy flux for various energies measured by ESA onboard THEMIS E, (b) the hot electron density N_h and total electron density inferred from spacecraft potential N_t, and (c) the ratio of hot electron density to total electron density (N_h/N_t). In Figure 2a, the white line indicates the minimum resonant energy for the whistler mode wave with a frequency of 0.5 f_{ce}.

A wave burst is defined as a recording lasting about 6–8 s, similar to the examples shown in Figure 1. During a wave burst, if whistler mode waves are observed, this wave burst is referred to as a wave event. In our database, the total number of wave events for rising tones, falling tones, and hiss-like emissions is 1310, 187, and 1688, respectively. For some wave events, in which both discrete (rising or falling tone) and hiss-like emissions coexist, we ignore the hiss-like wave and only regard them as the discrete (rising or falling tone) wave events, since the discrete emissions almost always have the dominant intensity compared to the coexisting hiss-like emissions in these events. For one wave event (lasting 6–8 s), at each recording time when the flag is consistent with its category, the wave amplitude B_w is calculated by

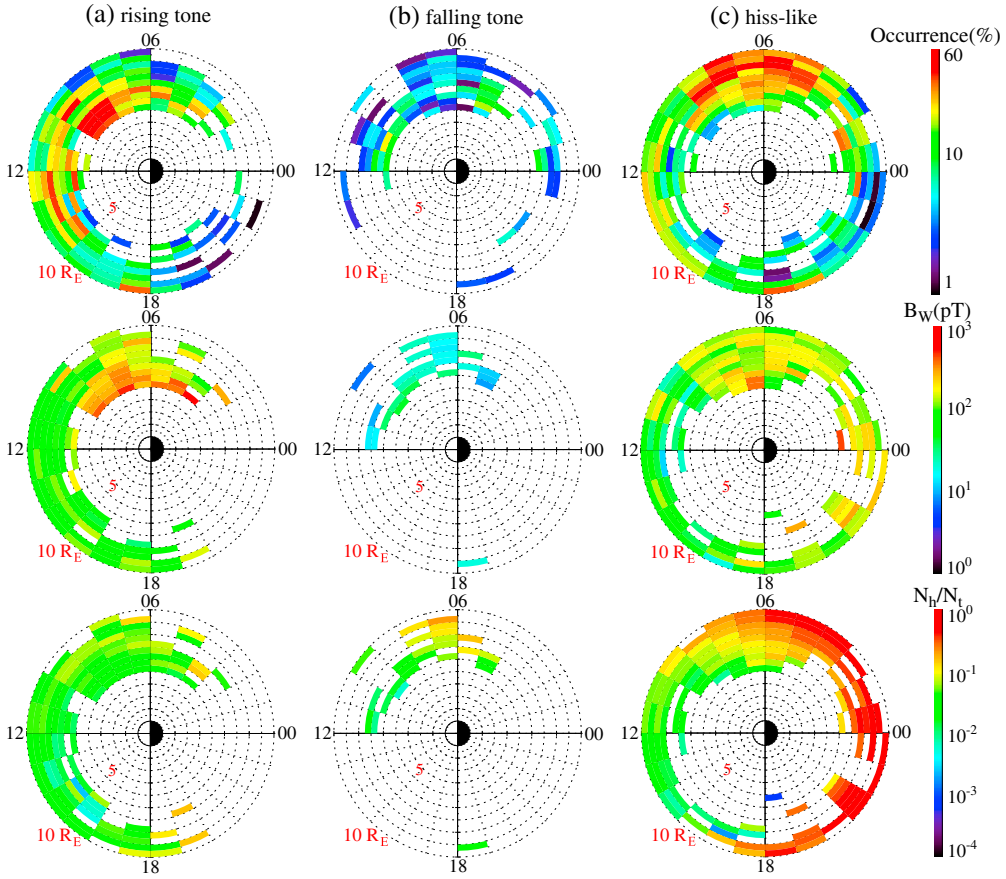

Figure 3. Global distribution of (top row) the occurrence rate, (middle row) wave amplitude B_w, and (bottom row) N_h/N_t in the L-MLT domain for three types of whistler mode wave emissions.

integrating the magnetic spectral density over the frequency from 0.1 to 0.5 f_{ce}. Subsequently, the wave power B_w^2 is averaged over the time when the corresponding wave emissions exist (the flag has a value of −1, 0, or 1) and used to characterize each wave event.

As mentioned above, the ratio of the hot electron density to the total electron density is closely related to the excitation of whistler mode waves. Figure 2 shows an example of how the ratio of hot to total electron density (N_h/N_t) is obtained. Figure 2a illustrates the time evolution of the electron flux as a function of energy measured by ESA onboard THEMIS E on 8 May 2013, where a white solid line indicates the minimum electron resonant energy, $E_{\min}$, for a wave frequency of 0.5 f_{ce}. This minimum electron resonant energy is given by $E_{\min} = (B_0^2/8\pi N_t)(f_{ce}/f)(1 - f/f_{ce})^3$ (where B_0 is the background magnetic field intensity) [*Kennel and Petschek*, 1966]. Then the density of hot electrons resonant with the lower band whistler mode waves is obtained by integrating the density over the energy from $E_{\min}$ to ~30 keV, which is the upper limit of the ESA energy channel, and is denoted by the red line in Figure 2b. The black line in Figure 2b indicates the total electron density, which is inferred from the spacecraft potential and the electron thermal speed and has an uncertainty generally within a factor of 2 [*Li et al.*, 2010]. However, this uncertainty does not affect our essential conclusion, since we evaluate the overall trend between the ratio of N_h/N_t and the whistler mode wave amplitude as discussed below. Finally, the ratio of hot electron density to total electron density is shown in Figure 2c. Note that the values of $E_{\min}$, N_t, N_h, and N_h/N_t in Figures 2a–2c are only shown in the region above 5 R_E, where our statistical analysis for the whistler mode waves was performed.

The global distribution of the occurrence rates, wave amplitudes, and N_h/N_t for the three wave categories in the L-MLT (magnetic local time) domain is illustrated in Figure 3 with a bin size of 0.5 L × 1 MLT. The color bar in the top row represents the occurrence rate, which is the ratio between the number of wave events in each bin and the number of the total wave bursts regardless of the presence of whistler mode

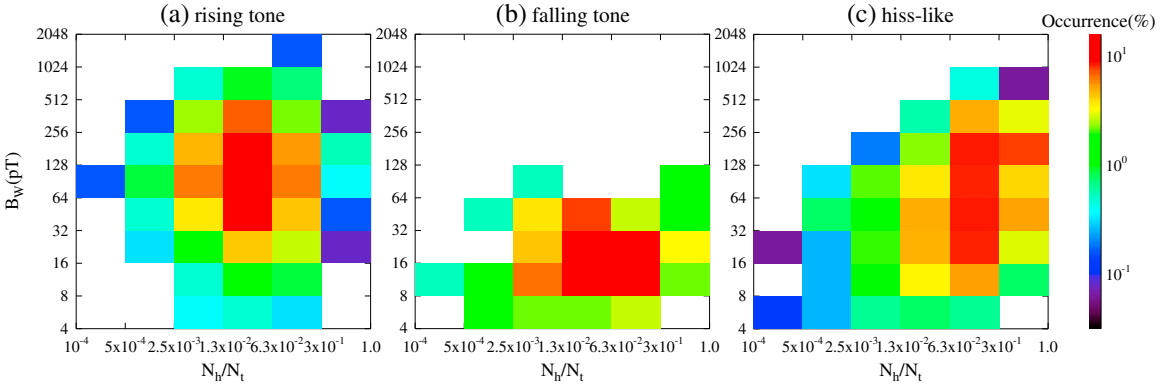

Figure 4. Distribution of the occurrence rate as a function of N_h/N_t and B_w for (a) rising tones, (b) falling tones, and (c) hiss-like emissions, respectively.

waves in the same bin. Note that the statistical significance on the nightside particularly at $<8\ R_E$ is limited due to the small number of wave bursts collected. The color bars in the middle row and bottom row represent the root-mean-square wave amplitude B_w and the mean value of N_h/N_t in each bin with more than two wave events. The global distribution of the occurrence rates for the three wave categories is generally consistent with previous results [*Li et al*., 2011a, 2012] and is shown here just as a reference. In the middle row, for rising and falling tones, the wave amplitude is large at low L shells and decreases with an increasing L shell. However, for the hiss-like emissions, the large wave amplitudes preferentially occur from the premidnight to the prenoon sector at nearly all L shells. Interestingly, for the hiss-like emissions, the region with the high N_h/N_t (bottom row) is nearly the same as that with the high wave amplitudes (middle row). Therefore, the wave amplitude of the hiss-like emission is likely to be closely correlated with N_h/N_t. However, there is no apparent correlation between B_w and N_h/N_t for the discrete emissions. As shown in the bottom row, the distribution of N_h/N_t for the rising and falling tones is almost uniform in the L-MLT region, where these emissions have finite occurrence rate, except for several bins with slightly larger values mostly near the dawn sector.

Figure 4 shows the distribution of wave events in the N_h/N_t and B_w domain for each category of whistler mode wave emission. The color bar indicates the occurrence rate in each bin, which is the ratio between the number of wave events in each bin and the total number of wave events in its corresponding category. In Figure 4a, it is clearly shown that rising tones have a very high occurrence rate in the region with N_h/N_t from 0.013 to 0.3 and the wave amplitude from 32 pT to 256 pT. However, when N_h/N_t or B_w is too small or too large, the occurrence rate is quite low. The same trend can also be found in Figure 4b. The falling tones usually have smaller wave amplitudes and preferentially occur in the region with N_h/N_t from 0.013 to 0.3 and the wave amplitude from 8 pT to 32 pT. However, for the hiss-like emissions, a very different trend is shown in Figure 4c. With the increase of N_h/N_t, the occurrence rate of hiss-like emissions generally increases, and the corresponding wave amplitudes become larger.

4. Conclusion and Discussion

We have utilized the waveform data from the THEMIS spacecraft to evaluate the global distribution of the wave amplitude B_w and the ratio of hot electron density to total electron density (N_h/N_t) for rising tones, falling tones, and hiss-like emissions, respectively. The preferential regions for the occurrence of the three types of emissions are further studied as a function of B_w and N_h/N_t in order to identify optimum excitation conditions for each category. For rising and falling tones, the wave amplitude is relatively large at low L shells ($<\sim8$) and decreases as the L shell increases. The corresponding distribution of N_h/N_t for rising and falling tones is almost uniform in the L-MLT domain. The rising (falling) tones are preferentially observed in the region with N_h/N_t from 0.013 to 0.3 and the wave amplitude from 32 pT to 256 pT (from 8 pT to 32 pT). However, for the hiss-like emissions, the waves with large amplitudes preferentially occur in the region where N_h/N_t is also high, extending from the nightside to the prenoon sector. Furthermore, with the increase of N_h/N_t, both the occurrence rates and wave amplitudes of hiss-like emissions generally increase.

For the hiss-like emissions, as shown in Figures 3 and 4, the wave amplitudes and occurrence rates are closely correlated with N_h/N_t. The correlation coefficient between $\log(B_w)$ and $\log(N_h/N_t)$ is about 0.33, indicating a fairly good correlation between them. This overall trend is consistent with the linear theory of whistler mode waves [*Kennel and Petschek*, 1966; *Li et al*., 2011b], where the linear growth rate is proportional to N_h/N_t. However, recent studies showed that hiss-like emissions can also be generated through nonlinear growth when the background magnetic field inhomogeneity is very small [*Katoh and Omura*, 2013; *Shoji and Omura*, 2014]. The relatively small correlation coefficient (~0.33) between $\log(B_w)$ and $\log(N_h/N_t)$ may be related to the fact that some of these hiss-like emissions are generated in the region with very small inhomogeneities, or other factors which are not discussed here (e.g., the anisotropy). In addition, a comparison of the frequency ranges obtained from the linear theory and observations would provide important clues for understanding the wave generation mechanisms, and an statistical survey of the correlation among the observed frequency ranges, wave amplitudes, and N_h/N_t would be an interesting extension of the present study.

However, for the discrete (rising and falling tones) emissions, there is no significant correlation between the wave amplitude and the N_h/N_t (Figures 3 and 4), and linear theory is not capable of explaining their properties. In addition, the correlation coefficients between $\log(B_w)$ and $\log(N_h/N_t)$ for rising and falling tones are 0.002 and 0.16, respectively. Interestingly, the discrete emissions preferentially occur in the region within a limited range in N_h/N_t. This supports the nonlinear wave growth theory [*Omura et al*., 2008, 2012], which suggests that an optimum amplitude of triggering waves is a key parameter of generating rising tone emissions [*Omura and Nunn*, 2011]. This optimum wave amplitude condition has also been confirmed by the self-consistent full particle simulations [*Hikishima and Omura*, 2012]. *Omura and Nunn* [2011] estimated the optimum wave amplitude for one rising tone event observed by Cluster at $L = 4.5$, which is about 100–500 pT according to Figure 6a in their paper. Their result is fairly close to our statistical result (32–256 pT), which was obtained from various locations with different plasma parameters.

Overall, our statistical results provide supporting experimental evidence for the nonlinear theory of generating rising tone chorus and also provide an important clue as to the generation mechanism of hiss-like emissions. Although the generation mechanism of falling tones, which typically have very oblique wave normal angles [e.g., *Li et al*., 2012], is still an open question, our statistical results suggest that their generation may not simply be explained by linear theory. Future investigation is needed to further explore their generation mechanism.

Acknowledgments

The work at UCLA was supported by the NASA grants NNX11AD75G, NNX11AR64G, NNX12AD12G, and NNX13AI61G. We acknowledge the THEMIS data obtained from http://themis.ssl.berkeley.edu/data/themis. The authors acknowledge A. Roux and O. LeContel for the use of SCM data; J.W. Bonnell and F.S. Mozer for the use of EFI data; and K.H. Glassmeier, U. Auster, and W. Baumjohann for the use of FGM data provided under the lead of the Technical University of Braunschweig and with the financial support through the German Ministry for Economy and Technology and the German Center for Aviation and Space (DLR) under contract 50 OC 0302. We would like to thank Judy Hohl for her help in editing the manuscript.

The Editor thanks George Hospodarsky and an anonymous reviewer for their assistance in evaluating this paper.

References

Angelopoulos, V. (2008), The THEMIS mission, *Space Sci. Rev.*, *141*(1–4), 5–34, doi:10.1007/s11214-008-9336-1.

Auster, H. U., et al. (2008), The THEMIS fluxgate magnetometer, *Space Sci. Rev.*, *141*, 235–264, doi:10.1007/s11214-008-9365-9.

Bonnell, J. W., F. S. Mozer, G. T. Delory, A. J. Hull, R. E. Ergun, C. M. Cully, V. Angelopoulos, and P. R. Harvey (2008), The Electric Field Instrument (EFI) for THEMIS, *Space Sci. Rev.*, *141*, 303–341, doi:10.1007/s11214-008-9469-2.

Bortnik, J., J. W. Cutler, C. Dunson, and T. E. Bleier (2007), An automatic wave detection algorithm applied to Pc1 pulsations, *J. Geophys. Res.*, *112*, A04204, doi:10.1029/2006JA011900.

Burtis, W. J., and R. A. Helliwell (1969), Banded chorus – A new type of Vlf radiation observed in the magnetosphere by OGO 1 and OGO 3, *J. Geophys. Res.*, *74*(11), 3002–3010, doi:10.1029/JA074i011p03002.

Cattell, C., et al. (2008), Discovery of very large amplitude whistler-mode waves in Earth's radiation belts, *Geophys. Res. Lett.*, *35*, L01105, doi:10.1029/2007GL032009.

Cully, C. M., J. W. Bonnell, and R. E. Ergun (2008), THEMIS observations of long-lived regions of large-amplitude whistler waves in the inner magnetosphere, *Geophys. Res. Lett.*, *35*, L17S16, doi:10.1029/2008GL033643.

Cully, C. M., V. Angelopoulos, U. Auster, J. Bonnell, and O. Le Contel (2011), Observational evidence of the generation mechanism for rising-tone chorus, *Geophys. Res. Lett.*, *38*, L01106, doi:10.1029/2010GL045793.

Helliwell, R. A. (1967), A theory of discrete VLF emissions from the magnetosphere, *J. Geophys. Res.*, *72*(19), 4773–4790, doi:10.1029/JZ072i019p04773.

Hikishima, M., and Y. Omura (2012), Particle simulations of whistler-mode rising-tone emissions triggered by waves with different amplitudes, *J. Geophys. Res.*, *117*, A04226, doi:10.1029/2011JA017428.

Horne, R. B., and R. M. Thorne (2003), Relativistic electron acceleration and precipitation during resonant interactions with whistler-mode chorus, *Geophys. Res., Lett.*, *30*(10), 1527, doi:10.1029/2003GL016973.

Horne, R. B., R. M. Thorne, S. A. Glauert, J. M. Albert, N. P. Meredith, and R. R. Anderson (2005), Timescale for radiation belt electron acceleration by whistler mode chorus waves, *J. Geophys. Res.*, *110*, A03225, doi:10.1029/2004JA010811.

Katoh, Y., and Y. Omura (2013), Effect of the background magnetic field inhomogeneity on generation processes of whistler-mode chorus and broadband hiss-like emissions, *J. Geophys. Res. Space Physics*, *118*, 4189–4198, doi:10.1002/jgra.50395.

Kennel, C. F., and H. E. Petschek (1966), Limit on stably trapped particle fluxes, *J. Geophys. Res.*, *71*, 1–28, doi:10.1029/JZ071i001p00001.

Koons, H. C., and J. L. Roeder (1990), A survey of equatorial magnetospheric wave activity between 5 and 8 R_E, *Planet. Space Sci.*, *38*(10), 1335–1341, doi:10.1016/0032-0633(90)90136-E.

Lauben, D. S., U. S. Inan, T. F. Bell, and D. A. Gurnett (2002), Source characteristics of ELF/VLF chorus, *J. Geophys. Res.*, *107*(A12), 1429, doi:10.1029/2000JA003019.

Le Contel, O., et al. (2008), First results of the THEMIS search coil magnetometers, *Space Sci. Rev.*, *141*(1–4), 509–534, doi:10.1007/s11214-008-9371-y.
LeDocq, M. J., D. A. Gurnett, and G. B. Hospodarsky (1998), Chorus source locations from VLF Poynting flux measurements with the Polar spacecraft, *Geophys. Res. Lett.*, *25*(21), 4063–4066, doi:10.1029/1998GL900071.
Li, W., R. M. Thorne, V. Angelopoulos, J. W. Bonnell, J. P. McFadden, C. W. Carlson, O. LeContel, A. Roux, K. H. Glassmeier, and H. U. Auster (2009), Evaluation of whistler-mode chorus intensification on the nightside during an injection event observed on the THEMIS spacecraft, *J. Geophys. Res.*, *114*, A00C14, doi:10.1029/2008JA013554.
Li, W., R. M. Thorne, J. Bortnik, Y. Nishimura, V. Angelopoulos, L. Chen, J. P. McFadden, and J. W. Bonnell (2010), Global distributions of suprathermal electrons observed on THEMIS and potential mechanisms for access into the plasmasphere, *J. Geophys. Res.*, *115*, A00J10, doi:10.1029/2010JA015687.
Li, W., R. M. Thorne, J. Bortnik, Y. Y. Shprits, Y. Nishimura, V. Angelopoulos, C. Chaston, O. Le Contel, and J. W. Bonnell (2011a), Typical properties of rising and falling tone chorus waves, *Geophys. Res. Lett.*, *38*, L14103, doi:10.1029/2011GL047925.
Li, W., R. M. Thorne, J. Bortnik, Y. Nishimura, and V. Angelopoulos (2011b), Modulation of whistler mode chorus waves: 1. Role of compressional Pc4-5 pulsations, *J. Geophys. Res.*, *116*, A06205, doi:10.1029/2010JA016312.
Li, W., R. M. Thorne, J. Bortnik, X. Tao, and V. Angelopoulos (2012), Characteristics of hiss-like and discrete whistler-mode emissions, *Geophys. Res. Lett.*, *39*, L18106, doi:10.1029/2012GL053206.
Macusova, E., et al. (2010), Observations of the relationship between frequency sweep rates of chorus wave packets and plasma density, *J. Geophys. Res.*, *115*, A12257, doi:10.1029/2010ja015468.
McFadden, J. P., C. W. Carlson, D. Larson, M. Ludlam, R. Abiad, B. Elliott, P. Turin, M. Marckwordt, and V. Angelopoulos (2008), The THEMIS ESA plasma instrument and in-flight calibration, *Space Sci. Rev.*, *141*(1–4), 277–302, doi:10.1007/s11214-008-9440-2.
Means, J. D. (1972), Use of 3-dimensional covariance matrix in analyzing polarization properties of plane waves, *J. Geophys. Res.*, *77*(28), 5551–5559, doi:10.1029/JA077i028p05551.
Meredith, N. P., R. B. Horne, and R. R. Anderson (2001), Substorm dependence of chorus amplitudes: Implications for the acceleration of electrons to relativistic energies, *J. Geophys. Res.*, *106*(A7), 13,165–13,178, doi:10.1029/2000JA900156.
Ni, B., R. M. Thorne, Y. Y. Shprits, and J. Bortnik (2008), Resonant scattering of plasma sheet electrons by whistler-mode chorus: Contribution to diffuse auroral precipitation, *Geophys. Res. Lett.*, *35*, L11106, doi:10.1029/2008GL034032.
Ni, B., R. M. Thorne, N. P. Meredith, Y. Y. Shprits, and R. B. Horne (2011), Diffuse auroral scattering by whistler mode chorus waves: Dependence on wave normal angle distribution, *J. Geophys. Res.*, *116*, A10207, doi:10.1029/2011ja016517.
Nishimura, Y., et al. (2010), Identifying the driver of pulsating aurora, *Science*, *330*(6000), 81–84, doi:10.1126/science.1193186.
Nishimura, Y., et al. (2013), Structures of dayside whistler-mode waves deduced from conjugate diffuse aurora, *J. Geophys. Res. Space Physics*, *118*, 664–673, doi:10.1029/201JA018242.
Omura, Y., and D. Nunn (2011), Triggering process of whistler mode chorus emissions in the magnetosphere, *J. Geophys. Res.*, *116*, A05205, doi:10.1029/2010JA016280.
Omura, Y., Y. Katoh, and D. Summers (2008), Theory and simulation of the generation of whistler-mode chorus, *J. Geophys. Res.*, *113*, A04223, doi:10.1029/2007JA012622.
Omura, Y., D. Nunn, and D. Summers (2012), Generation processes of whistler mode chorus emissions: Current status of nonlinear wave growth theory, in *Dynamics of the Earth's Radiation Belts and Inner Magnetosphere*, edited by D. Summers et al., *Geophys. Monogr. Ser.*, vol. 199, pp. 243–254, AGU, Washington, D. C., doi:10.1029/2012gm001347.
Roux, A., O. Le Contel, C. Coillot, A. Bouabdellah, B. de la Porte, D. Alison, S. Ruocco, and M. C. Vassal (2008), The search coil magnetometer for THEMIS, *Space Sci. Rev.*, *141*(1–4), 265–275, doi:10.1007/s11214-008-9455-8.
Santolik, O., D. A. Gurnett, J. S. Pickett, M. Parrot, and N. Cornilleau-Wehirlin (2005), Central position of the source region of storm-time chorus, *Planet. Space Sci.*, *53*, 299–305, doi:10.1016/j.pss.2004.09.056.
Santolik, O., E. Macusova, E. E. Titova, B. V. Kozelov, D. A. Gurnett, J. S. Pickett, V. Y. Trakhtengerts, and A. G. Demekhov (2008), Frequencies of wave packets of whistler-mode chorus inside its source region: A case study, *Ann. Geophys.*, *26*(6), 1665–1670.
Shoji, M., and Y. Omura (2014), Spectrum characteristics of electromagnetic ion cyclotron triggered emissions and associated energetic proton dynamics, *J. Geophys. Res. Space Physics*, *119*, 3480–3489, doi:10.1002/2013JA019695.
Summers, D., R. M. Thorne, and F. L. Xiao (1998), Relativistic theory of wave-particle resonant diffusion with application to electron acceleration in the magnetosphere, *J. Geophys. Res.*, *103*(A9), 20,487–20,500, doi:10.1029/98JA01740.
Tao, X., W. Li, J. Bortnik, R. M. Thorne, and V. Angelopoulos (2012), Comparison between theory and observation of the frequency sweep rates of equatorial rising tone chorus, *Geophys. Res. Lett.*, *39*, L08106, doi:10.1029/2012GL051413.
Thorne, R. M., T. P. O'Brien, Y. Y. Shprits, D. Summers, and R. B. Horne (2005), Timescale for MeV electron microburst loss during geomagnetic storms, *J. Geophys. Res.*, *110*, A09202, doi:10.1029/2004JA010882.
Thorne, R. M., B. B. Ni, X. Tao, R. B. Horne, and N. P. Meredith (2010), Scattering by chorus waves as the dominant cause of diffuse auroral precipitation, *Nature*, *467*(7318), 943–946, doi:10.1038/Nature09467.
Thorne, R. M., et al. (2013), Rapid local acceleration of relativistic radiation-belt electrons by magnetospheric chorus, *Nature*, *504*(7480), 411, doi:10.1038/Nature12889.
Trakhtengerts, V. Y. (1995), Magnetosphere cyclotron maser: Backward wave oscillator generation regime, *J. Geophys. Res.*, *100*(A9), 17,205–17,210, doi:10.1029/95JA00843.
Tsurutani, B. T., and E. J. Smith (1974), Postmidnight chorus - substorm phenomenon, *J. Geophys. Res.*, *79*(1), 118–127, doi:10.1029/Ja079i001p00118.
Tsurutani, B. T., and E. J. Smith (1977), Two types of magnetospheric ELF chorus and their substorm dependences, *J. Geophys. Res.*, *82*(32), 5112–5128, doi:10.1029/Ja082i032p05112.
Tsurutani, B. T., O. P. Verkhoglyadova, G. S. Lakhina, and S. Yagitani (2009), Properties of dayside outer zone chorus during HILDCAA events: Loss of energetic electrons, *J. Geophys. Res.*, *114*, A03207, doi:10.1029/2008JA013353.